

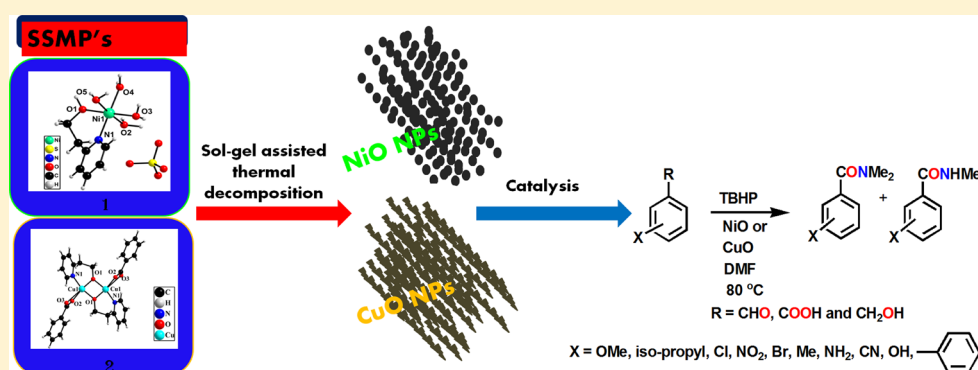
Facile Access to Amides from Oxygenated or Unsaturated Organic Compounds by Metal Oxide Nanocatalysts Derived from Single-Source Molecular Precursors

Akbar Mohammad,[†] Prakash Chandra,[‡] Topi Ghosh,[†] Mauro Carraro,[⊥] and Shaikh M. Mobin^{*,†,‡,§,Ⓜ}

[†]Discipline of Chemistry, [‡]Discipline of Metallurgy Engineering and Materials Science (MEMS), and [§]Centre for Biosciences and Bio-Medical Engineering, Indian Institute of Technology (IIT) Indore, Simrol, Khandwa Road, Indore 453552, India

[⊥]Department of Chemical Sciences, University of Padova and ITM-CNR, Via Marzolo 1, 35131 Padova, Italy

Supporting Information



ABSTRACT: Oxidative amidation is a valuable process for the transformation of oxygenated organic compounds to valuable amides. However, the reaction is severely limited by the use of an expensive catalyst and limited substrate scope. To circumvent these limitations, designing a transition-metal-based nanocatalyst via more straightforward and economical methodology with superior catalytic performances with broad substrate scope is desirable. To resolve the aforementioned issues, we report a facile method for the synthesis of nanocatalysts NiO and CuO by the sol–gel-assisted thermal decomposition of complexes [Ni(hep-H)(H₂O)₄SO₄] (SSMP-1) and [Cu(μ-hep)(BA)]₂ (SSMP-2) [hep-H = 2-(2-hydroxyethyl)pyridine; BA = benzoic acid] as single-source molecular precursors (SSMPs) for the oxidative amidation of benzyl alcohol, benzaldehyde, and BA by using *N,N*-dimethylformamide (DMF) as the solvent and as an amine source, in the presence of *tert*-butylhydroperoxide (TBHP) as the oxidant, at *T* = 80 °C. In addition to nanocatalysts NiO and CuO, our previously reported Co/CoO nanocatalyst (CoNC), derived from the complex [Co^{II}(hep-H)(H₂O)₄SO₄] (A) as an SSMP, was also explored for the aforementioned reaction. Also, we have carefully investigated the difference in the catalytic performance of Co-, Ni-, and Cu-based nanoparticles synthesized from the SSMP for the conversion of various oxygenated and unsaturated organic compounds to their respective amides. Among all, CuO showed an optimum catalytic performance for the oxidative amidation of various oxygenated and unsaturated organic compounds with a broad reaction scope. Finally, CuO can be recovered unaltered and reused for several (six times) cycles without any loss in catalytic activity.

■ INTRODUCTION

The amide functionality is ubiquitous in life and plays a critical role in virtually all biological processes. The amide bond is prevalent in most biomolecules, and it is consistently found as a cardinal structural element in several fine chemicals, pharmaceuticals, and agrochemicals.^{1,2} Moreover, polymers based on the amide linkage, such as polyamides (nylons, Kevlar), play a pivotal role in a wide range of applications, including drug delivery, wound healing, and adhesive fabrication.^{3,4} Activation of a carboxylic acid and subsequent coupling of the activated species with an amine is predominantly utilized for amide synthesis.^{3,5} However, there are several other methods for the introduction of an amide functional group, such as hydration of

nitriles, aminocarbonylation of aryl halides,^{6,7} rearrangement of oximes,⁸ amidation of aryl halides using isocyanides,⁹ carbonylative synthesis from alkanes, primary amines, and CO,¹⁰ and oxidative amidation of alcohols with amines.¹¹

The development of a highly efficient and environmentally sound methodology for the synthesis of amides, from inexpensive and abundant feedstocks, is highly desirable both in academic research and for industrial applications.^{3,6,7} Recently, the use of straightforward methodologies for the direct amination of nitriles,¹² carboxylic acids,¹³ aldehydes,¹⁴

Received: June 20, 2017

Published: August 21, 2017



methylarenes,¹⁵ aryl esters,^{8,16} and alcohols,¹⁷ has become a topical area of research. The procedures consist of CO-free oxidative couplings with *N,N*-dialkylformamides; for example, *N,N*-dialkylated amides were synthesized using nitriles and *N,N*-dimethylformamide (DMF) or diethylformamide under an O₂ atmosphere, in the presence of Cu₂O and 1,10-phenanthroline.¹⁸ Li et al.¹⁴ used a Co-based catalyst on carbonized organic ligands (Co@C–N) and DMF, obtaining an excellent catalytic performance for the transformation of aldehydes into *N*-alkylated amides in the presence of *tert*-butylhydroperoxide (TBHP) as the oxidant. Zhaorigetu et al.¹⁶ reported the catalytic transformation of aromatic and heteroaromatic esters to *N*-alkylated amides using a nanosized palladium catalyst, *N,N*-dialkylformamides, and TBHP. However, despite considerable accomplishments in amide formation, all of these reactions are often associated with some limitations, such as the use of less available starting materials, expensive noble metal catalysts or ligands, need for harsh reaction conditions, use of toxic solvents, and massive production of waste.^{12,18,19}

The relatively new concept of using single-source molecular precursor (SSMP), for the preparation of novel catalytic species, can be helpful to overcome these issues. In particular, single-source approaches involve the use of an organometallic or metal–organic molecule as a precursor for the synthesis of transition-metal/metal oxide-based nanoparticles.^{20,21} SSMPs provide several key advantages over other routes because they are air-stable, nontoxic, and easy to handle. Moreover, they employ clean, low-temperature decomposition routes and yield crystalline nanomaterials with minimal impurity incorporation.²²

Transition-metal/metal oxide nanoparticles prepared by SSMPs have been used in catalysis^{23,24} as well as in sensing²⁵ and for the preparation of electrochromic materials.²⁶ For example, Co₃O₄ nanorods prepared by the precipitation of cobalt acetate using sodium carbonate have been utilized for low-temperature CO oxidation.²⁷ Monodispersed Ni and NiO nanoparticles synthesized by reduction of the nickel oleylamine complex were utilized for Suzuki coupling reaction.²⁸ The cobalt/cobalt oxide nanocatalyst (Co/CoO or CoNC), synthesized by reduction of the cobalt complex [Co^{II}(hep-H)(H₂O)₄]SO₄ (A; hep-H = 2-(2-hydroxyethyl)pyridine), was used for the selective reduction of polyaromatic nitro compounds to their respective amines under ambient conditions, using NaBH₄ as a reducing agent.²⁹ (PrO)₂Ta[OSi(O^tBu)₃]₃ and [(^tBuO)₂Ti{μ-O₂Si[OSi(O^tBu)₃]₂}]₂ were utilized as SSMPs to prepare Ta₂O₅·*x*SiO₂³⁰ and Ti^{IV}/SiO₂,³¹ respectively, which were used to obtain selective cyclohexene epoxidation.

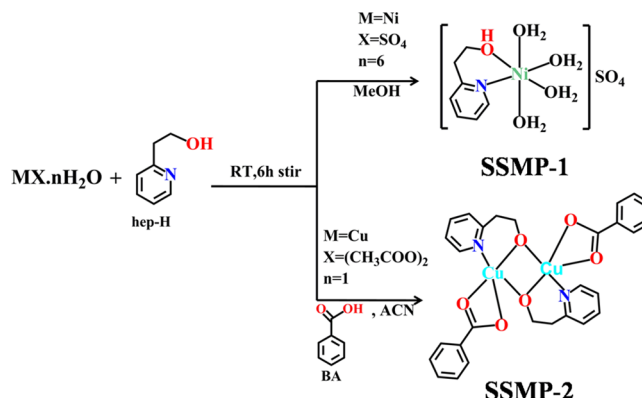
Herein, we have investigated the synthesis of *N*-alkylated amides starting from alcohols, aldehydes, acids, and unsaturated compounds using DMF as the solvent as well as the amine source, in the presence of cobalt, nickel, and copper oxide-based nanocatalysts, obtained by their respective SSMPs.

RESULTS AND DISCUSSION

Synthesis of SSMPs. The reaction of NiSO₄·6H₂O with hep-H in methanol (MeOH) and Cu(CH₃COO)₂·H₂O, hep-H, and benzoic acid (BA) in acetonitrile at room temperature yielded the SSMPs [Ni^{II}(hep-H)(H₂O)₄]SO₄ (SSMP-1) and [Cu^{II}(μ-hep)(BA)]₂ (SSMP-2) (Scheme 1).

The synthesis and characterization of CoNC by employing a SSMP was recently reported by us.^{29,32} Two new nanocatalysts, NiO and CuO, have been obtained by the sol–gel-assisted

Scheme 1. Synthesis of SSMP-1 and SSMP-2



thermal decomposition of their respective SSMP-1 and SSMP-2, in an aqueous solution within the pH range of 2.0–2.5, using citric acid (1.0 M) as the proton source as well as stabilization of the nanoparticles and control of their nucleation during thermal decomposition of the molecular precursor (Figure 1).³³

Molecular Structures of SSMP-1 and SSMP-2. The molecular structures of SSMP-1 and SSMP-2 were authenticated by their single-crystal X-ray diffraction (XRD) studies. SSMP-1 crystallizes in the noncentrosymmetric, monoclinic, *P*2₁ space group (Table S1). The asymmetric unit of SSMP-1 consists of one Ni^{II} ion, one bidentate hep-H ligand, and four-coordinated water molecules. The overall charge on SSMP-1 was balanced by the counterion SO₄²⁻. The N and O atoms from hep-H and two coordinated water molecules constitute the basal plane, and the remaining two water molecules occupy the axial position with elongated bond lengths, forming a distorted octahedral geometry all over the Ni^{II} ion. SSMP-2 crystallizes in the centrosymmetric, triclinic, *P* $\bar{1}$ space group with two half-molecules in an asymmetric unit (Table S1). Each Cu^{II} ion in the dimeric unit is in the five-coordinated NO₄ environment, where the basal plane consists of one O atom from BA, two O atoms [bis(μ₂-O)], and one N atom from the hep⁻ ligand, while the remaining site is occupied by another O atom of BA with an elongated bond length, thus yielding a distorted square-pyramidal geometry. The perspective views of SSMP-1 and SSMP-2 are shown in Figure 1.

Characterization of the Nanocatalysts (NiO and CuO).

The nanocatalysts NiO and CuO were fully characterized by various physicochemical techniques, such as powder XRD, transmission electron microscopy (TEM), selected-area electron diffraction (SAED), field-emission scanning electronic microscopy (FESEM), energy-dispersive X-ray spectroscopy (EDAX), and X-ray photoelectron spectroscopy (XPS).

The crystallinity and phase purity of the NiO and CuO nanocatalysts were determined by XRD spectra and are shown in Figure 2. The XRD patterns clearly show the formation of NiO nanoparticles with 2θ = 37.2°, 43.3°, 62.9°, 75.4°, and 79.3°, which can be readily indexed as the 111, 200, 220, 311, and 222 crystal planes of bulk NiO, having a face-centered-cubic NiO phase (JCPDS 71-1179).³⁴ The crystalline nature of the sample was further confirmed by the sharpness and intensity of the peaks of the synthesized sample. The average crystallite size of the nanoparticles was determined using the Scherrer equation.³⁵

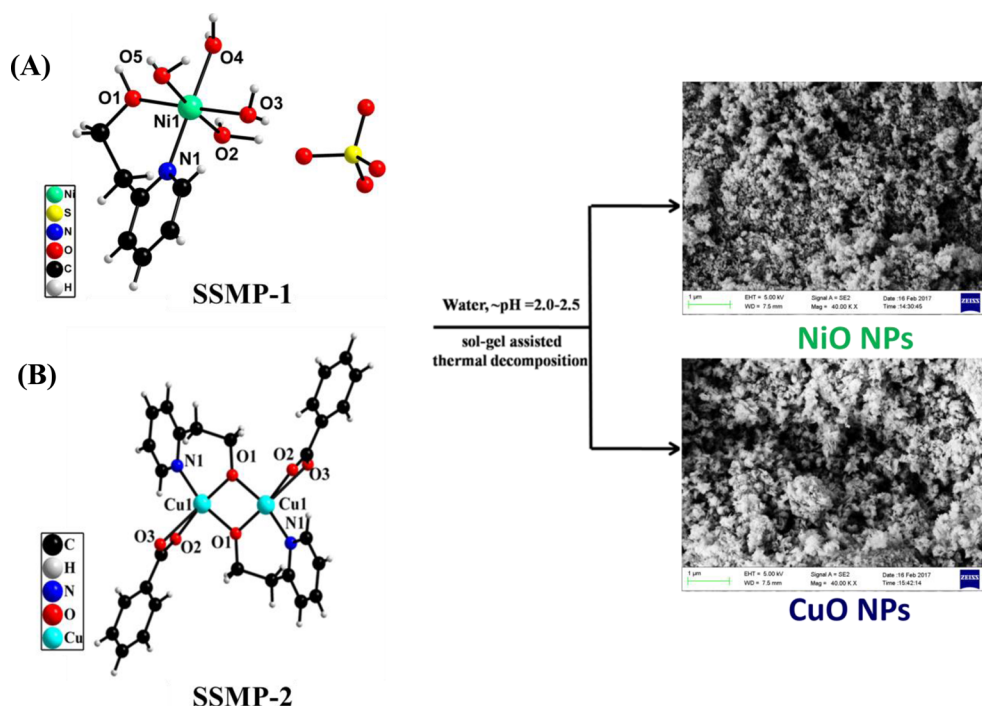


Figure 1. Preparation of NiO (A) and CuO (B) nanocatalysts from SSMP-1 and SSMP-2. Perspective views show the molecular structures of SSMP-1 and SSMP-2 (the other molecule in the asymmetric unit of SSMP-2 has been omitted for clarity), while SEM images show the morphology of the nanocatalysts.

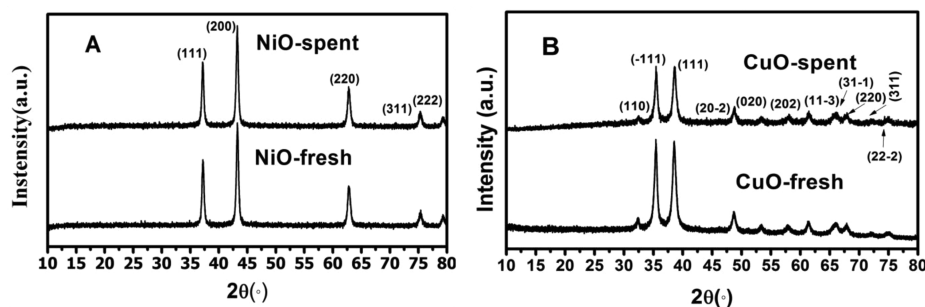


Figure 2. XRD spectra of fresh and spent NiO (A) and CuO (B) nanocatalysts.

$$B(2\theta) = \frac{K\lambda}{L \cos \theta}$$

The average crystallite size of the NiO nanoparticles was found to be 20.6 nm. No peak due to $\text{Ni}(\text{OH})_2$ was observed by XRD. The XRD pattern of the CuO nanoparticles showed monoclinic structures with $2\theta = 32.3^\circ, 35.4^\circ, 38.5^\circ, 48.7^\circ, 53.4^\circ, 57.9^\circ, 61.5^\circ, 66.1^\circ, 67.9^\circ, 72.1^\circ$, and 75.2° , which can be readily indexed as 110, -111 , 111, $20-2$, 020, 202, $11-3$, $31-1$, 220, 311, and $22-2$ planes (JCPDS 48-1548).³⁶ The average crystallite size of the CuO nanoparticles was found to be 13.8 nm. Additionally, we have also performed XRD for spent catalysts (NiO and CuO), which show no additional peaks, confirming the purity of the catalyst used.

The size and morphology of the NiO and CuO nanocatalysts were characterized using FESEM and high-resolution TEM (HRTEM). FESEM and HRTEM photomicrographs of the NiO nanocatalyst showed spherical shape having approximately ~ 20 – 30 nm diameter with smooth and uniform morphology (Figures 1, 3A–C, and S3A–C). The SAED pattern of NiO obtained from HRTEM showed a concentric ring pattern,

indicating the crystalline nature (bright spots) of NiO (Figure 3D). SEM–EDAX analysis of fresh and spent catalysts showed not many changes in the morphological characteristics (Figures S3A–C and S4A–C), while Ni and O atoms in the same atomic ratio confirmed that there was no leaching of nickel from the catalyst surface (Figures S3D and S4D).

SEM and HRTEM analysis of the CuO nanocatalyst confirmed that the rod-shaped morphology may be due to the agglomeration of several crystallites with widths of approximately ~ 10 – 15 nm and lengths of ~ 100 – 150 nm (Figures 4A–C and S5A–C). The SAED pattern obtained from HRTEM for the CuO nanocatalyst showed a concentric ring pattern, indicating the crystalline nature of the material (Figure 4D). Similarly, SEM–EDAX analysis of fresh and spent CuO catalysts also showed not many changes in the morphological characteristics (Figures 1 and S5A–C and S6A–C) and confirmed that there was no leaching of the metal from the copper oxide nanoparticle surface (Figures S5D and S6D).

Further, XPS analysis was performed to obtain the elemental composition and chemical and electronic states of the CoNC,

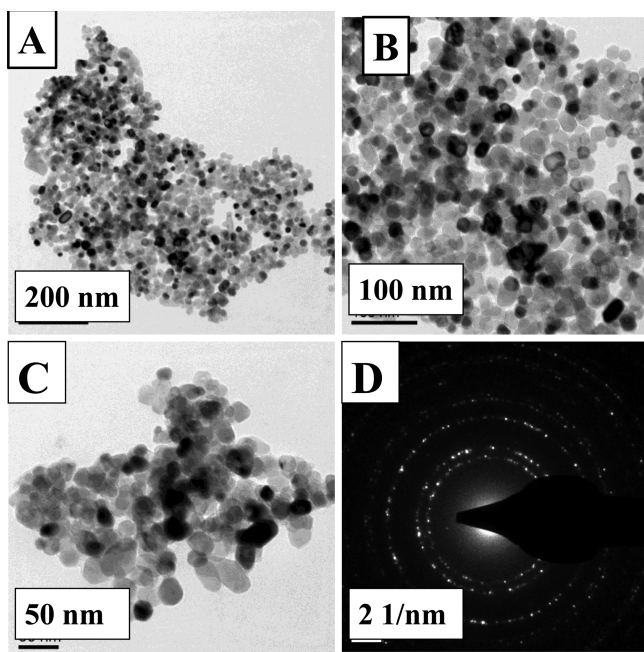


Figure 3. HRTEM images of the NiO nanocatalysts with 200 nm (A), 100 nm (B), 50 nm (C) scale bars, and SAED pattern at 2 1/nm (D).

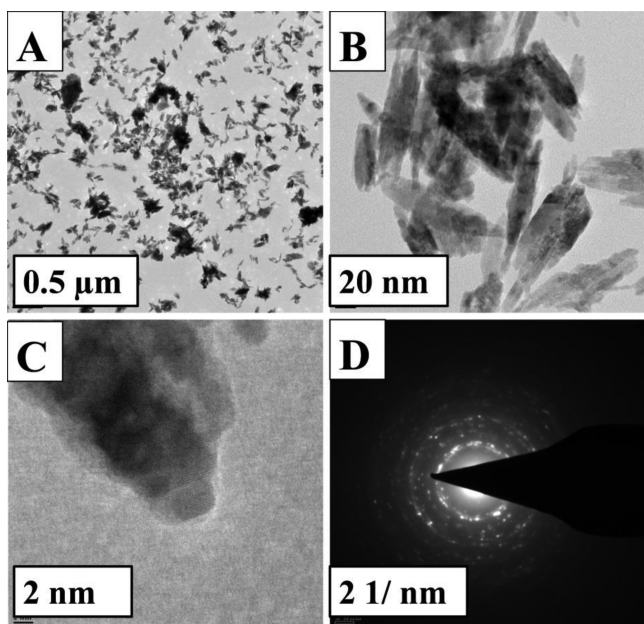


Figure 4. HRTEM images of the CuO nanocatalyst with 0.5 μm (A), 20 nm (B), 2 nm (C) scale bars, and SAED pattern at 2 1/nm (D).

NiO, and CuO nanocatalysts. All of the binding energies were calibrated using the C 1s peak at 284.6 eV. The XPS spectra of CoNC were discussed in our previous report.²⁹ The Ni 2p region comprises four easily discernible features: the Ni 2p_{3/2} main peak and its satellites at ~ 853 and ~ 859 eV and the Ni 2p_{1/2} main peak at ~ 872 eV (Figure S5).³⁷ XPS spectra were also collected after five catalytic recycles, showing identical spectra for the fresh and spent catalysts, clearly indicating that there was no change in the oxidation state of Ni²⁺. The peak at ~ 530 eV (Figure S7B,D) represents O 1s spectra of the fresh and spent NiO nanocatalysts. XPS analysis also confirmed the absence of Ni⁰ in both fresh and spent catalysts.

The Cu 2p peak of the XPS spectrum of CuO is shown in Figure 6; the two peaks centered at 933 and 953 eV were assigned to Cu 2p_{3/2} and Cu 2p_{1/2} of CuO, respectively. The presence of two extra shakeup satellite peaks at relatively higher binding energies, 943 eV, also indicate the existence of CuO on the surface.^{36,38} The XPS spectra of fresh and spent catalysts were identical, clearly indicating that there was no change in the oxidation state of Cu²⁺ even after six recycles. The peak at ~ 530 eV (Figure S7F,H) represents O 1s spectra of the fresh and spent CuO nanocatalysts. XPS analysis also confirmed the absence of Cu⁰ in the fresh and spent CuO nanocatalysts.

Catalytic Activity of the Nanocatalysts. Catalytic oxidative amidation of oxygenated organic compounds (alcohols, aldehydes, and acids) was carried out by the series of nanocatalysts CoNC, NiO, and CuO employing DMF as the solvent and TBHP as the oxidative reagent at a temperature of 80 °C (see Chart 1), as optimized by Li et al.¹⁴ CoNC gave moderate conversion of benzyl alcohol (78%) with a poor selectivity (25%) for the desired product, *N,N*-dimethylbenzamide (1). With benzaldehyde, a 77% conversion was observed without any formation of 1, while *N*-methylbenzamide (2) was obtained with 18% selectivity. BA (4) was formed as a major product with 71% selectivity. Under identical reaction conditions, without using the catalyst, no reaction was observed, hence confirming that the reaction was truly catalytic. Similarly, NiO resulted in 83% conversion of benzyl alcohol, but with only 8% and 20% selectivity for 1 and 2, respectively, and 49% selectivity for 4. With benzaldehyde, an improved catalytic performance was observed, with 92% conversion and 50%, 11%, and 21% selectivity for 1, 2, and 4. Both CoNC and NiO showed poor catalytic performance with BA, with 5% and 8% conversion, respectively. On the contrary, the CuO nanocatalyst effectively catalyzed the oxidative amidation of benzyl alcohol, benzaldehyde, and BA with 92%, 91%, and 100% conversion, respectively, and their selectivities for 1 were 72%, 89%, and 100%, respectively (see Chart 1). The isolated yield was obtained with the help of column chromatography for the oxidative amidation of benzyl alcohol, benzaldehyde, and BA to 1. The yields of benzyl alcohol, benzaldehyde, and BA were found to be 95 mg (64%), 115 mg (77%), and 145 mg (97%), respectively. The isolated yields obtained from column chromatography are thus close to those obtained from gas chromatography–mass spectrometry (GC–MS). Commercially available CuO was also investigated for catalytic performance for the oxidative amidation of benzaldehyde. The catalytic reaction results showed 78% benzaldehyde conversion with 57% selectivity for 1, clearly showing that CuO prepared from SSMP-2 showed a better catalytic performance compared to the commercially available CuO.

The order of effectiveness of nanocatalysts in catalyzing the oxidative amidation of alcohols, aldehydes, and acids was thus found to be CuO > NiO > CoNC (Chart 1).

A comparative study of Co-, Ni-, and Cu-based nanoparticles and their respective SSMPs was performed. For benzyl alcohol, Co- and Ni-based SSMPs showed 75% and 60% conversion of benzyl alcohol and 45% and 50% selectivity for 1, respectively. For benzaldehyde, similar catalytic performances were obtained with both Co- and Ni-based SSMPs. These showed better catalytic activity for BA with 62% and 57% conversion and 58% and 70% selectivity for 1, respectively. In this case, the lower reactivity of Co- and Ni-based nanocatalysts may be due to the decreased availability of active sites.

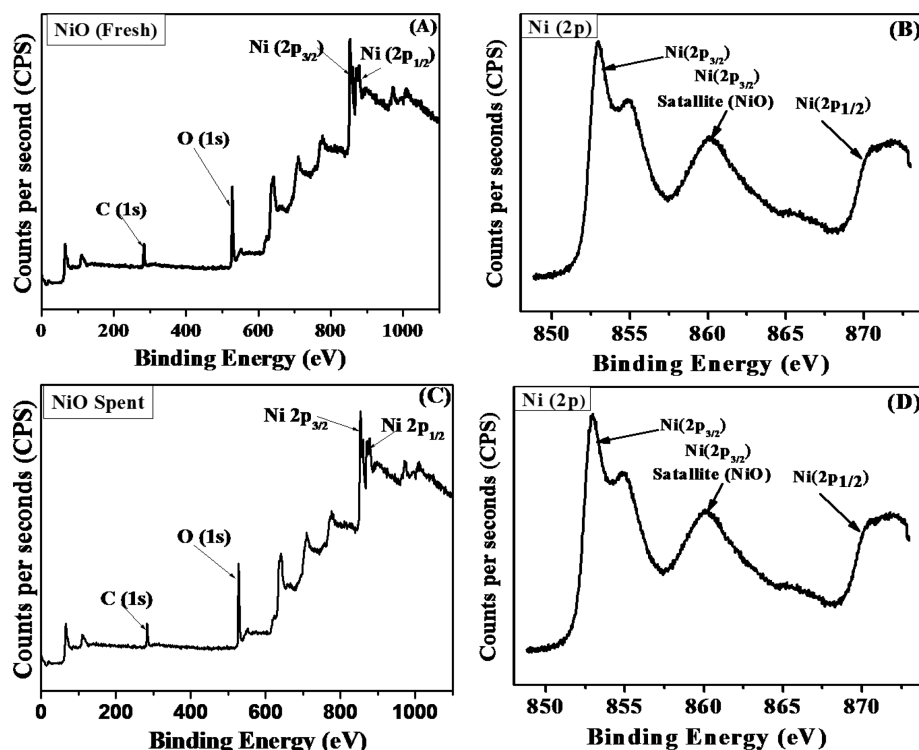


Figure 5. XPS spectra of (A) fresh NiO, (B) Ni present in NiO, (C) spent NiO, and (D) Ni present in spent NiO.

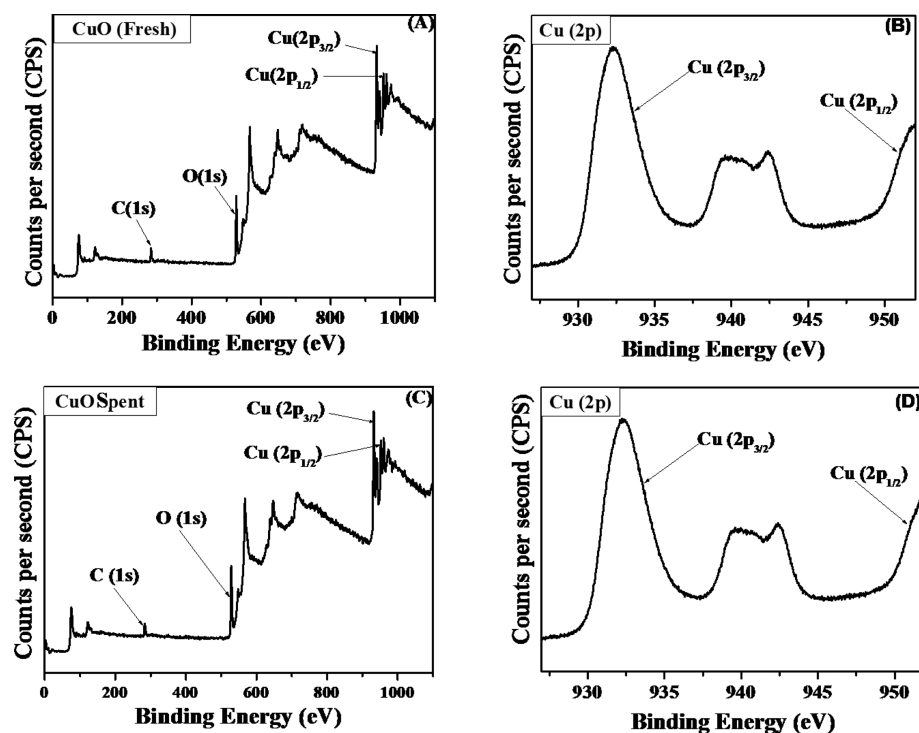


Figure 6. XPS spectra of (A) fresh CuO, (B) Cu present in CuO, (C) spent CuO, and (D) Cu present in spent CuO.

SSMP-2 showed 100%, 76%, and 96% conversion of benzyl alcohol, benzaldehyde, and BA, respectively, with 43%, 69%, and 72% selectivity for **1**. The comparative study for Cu-based SSMP-2 and CuO nanoparticles shows that the CuO displays higher conversion of benzaldehyde, benzyl alcohol, and BA and higher selectivity for **1**. The outcome of the comparative catalytic performance also shows that CuO nanoparticles

outperform the other transition-metal-based nanoparticles for the catalytic oxidative amidation of oxygenated hydrocarbons, confirming their superior performance (Chart 2). Further, CuO shows excellent recyclability, easily separable nature, and higher selectivity compared to SSMPs and the other nanocatalysts discussed above.

Chart 1. Comparative Studies for the Reaction of Benzyl Alcohol, Benzaldehyde, and BA by Employing CoNC, NiO, and CuO Nanocatalysts^a

	R = CH ₂ OH	% Conv = 78	(1)	(2)	(3)	(4)	Others
			25.2	--	--	35	39.8
		%Select					
	R = CHO	% Conv = 77	--	18	--	71	11
		%Select					
	R = COOH	% Conv = 5	22.8	34	--	--	43.2
		%Select					
	R = CH ₂ OH	% Conv = 83.4	(1)	(2)	(3)	(4)	Others
			7.8	19.8	--	49	23.4
		%Select					
	R = CHO	% Conv = 92	50	11.3	--	21	17.7
		%Select					
	R = COOH	% Conv = 8	67	4.8	--	--	28.2
		%Select					
	R = CH ₂ OH	% Conv = 91.9	(1)	(2)	(3)	(4)	Others
			71.5	--	--	11.3	17.2
		%Select					
	R = CHO	% Conv = 90.6	89	--	--	8	3
		%Select					
	R = COOH	% Conv = 100	100	--	--	--	--
		%Select					
	R = CHO	% Conv > 78%	(1)	(2)	(3)	(4)	Others
			57	18	21	3	1
		%Select					

^aReaction conditions: substrate = 1 mmol; TBHP = 6 equiv; catalyst = 10 mg; DMF = 2 g (2.12 mL); *T* = 80 °C; reaction time = 20 h. The substrate conversion and product selectivity were determined by GC–MS.

Probable Mechanism for an N-Alkylated Amide from Alcohols, Aldehydes, and Acids. According to a previous report, oxidative amidation in the presence of transition metals such as Co-, Ni-, or Cu-based oxides proceeds via the radical-chain mechanism (Scheme 2).³⁹ Catalytic oxidative amidation of alcohols or aldehydes begins with the activation of TBHP by CoNC, NiO, or CuO via the formation of radicals I and II (Scheme 2A). In the case of alcohol, TBHP in the presence of CoNC, NiO, or CuO fosters its oxidation to the aldehyde. Further, the resulting aldehyde molecule reacts with I or II to

Chart 2. Comparative Studies for the Reaction of Benzyl Alcohol, Benzaldehyde, and BA by Employing Co-, Ni-, and Cu-Based SSMPs^a

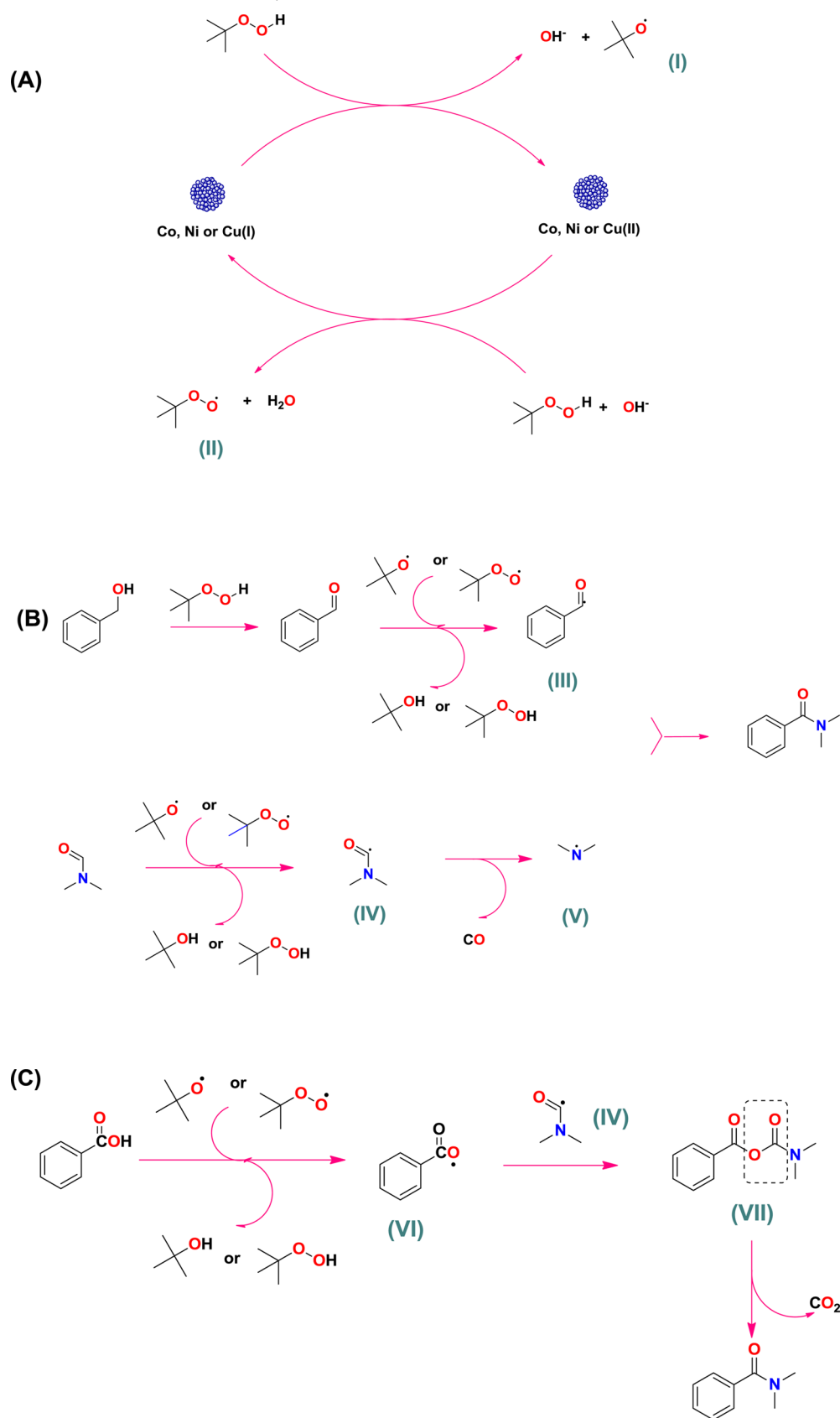
	R = CH ₂ OH	% Conv = 75.2	(1)	(2)	(3)	(4)	Others
			45	14	2	37	2
		%Select					
	R = CHO	% Conv = 73	64	24	--	11	1
		%Select					
	R = COOH	% Conv = 62	58	40	--	--	2
		%Select					
	R = CH ₂ OH	% Conv = 60	(1)	(2)	(3)	(4)	Others
			50	33	--	5	12
		%Select					
	R = CHO	% Conv = 74	61	6	--	13	20
		%Select					
	R = COOH	% Conv = 57	70	22.7	--	--	6.3
		%Select					
	R = CH ₂ OH	% Conv = 100	(1)	(2)	(3)	(4)	Others
			43	12	43	1	1
		%Select					
	R = CHO	% Conv = 76	69	25	--	8	3
		%Select					
	R = COOH	% Conv = 96	72	22	--	4.7	1.3
		%Select					

^aReaction conditions: substrate = 1 mmol; TBHP = 6 equiv; SSMPs as the catalyst = 10 mg; DMF = 2 g (2.12 mL); *T* = 80 °C; reaction time = 20 h. The substrate conversion and product selectivity were determined by GC–MS.

form III; simultaneously, the DMF molecule reacts with I or II to form IV and V. Finally, III and V react to form the desired N-alkylated amide. It is worth noting that no intermediate benzaldehyde can be observed along with the other products. A similar pathway is also possible when using aldehyde as the starting material (Scheme 2B).

Carboxylic acid follows a slightly divergent mechanism compared to the corresponding alcohols or aldehydes. The experimental results reveal that CoNC and NiO show poor catalytic performance with carboxylic acid, probably because of their inefficiency in activating the same to form VI. CuO, on the other hand, effectively catalyzes the generation of VI from the carboxylic acid molecule, therefore showing superior catalytic performance compared to CoNC and NiO. In situ generated IV and VI react with each other to form VII. In conclusion, VII loses a carbon dioxide molecule to form the desired N-alkylated amide (Scheme 2C). The formation of *tert*-butyl benzoperoxoate as a major intermediate^{13,39} has been ruled out by a control experiment, involving the use of this

Scheme 2. Reaction Mechanism for Synthesis of *N*-Alkylated Amide from Alcohols, Aldehydes, and Acids Using DMF in the Presence of CoNC, NiO, and CuO Nanocatalysts

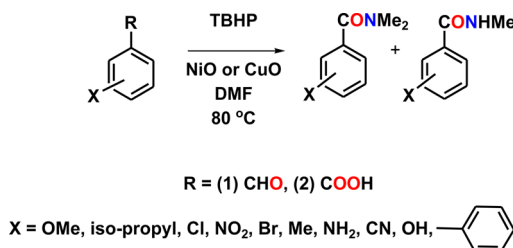


peroxoester as a substrate under identical conditions (Chart S1). This latter, indeed, was quantitatively converted to a mixture

containing *N,N*-dimethylbenzamide (56% selectivity) and *N*-methylbenzamide (30% selectivity).

These interesting results further encouraged us to broaden the substrate scope, including the catalytic oxidative amidation of substituted derivatives of benzaldehyde and BA and of five-membered ring reactants (Scheme 3, Tables 1 and 2), under

Scheme 3. Catalytic Oxidative Amidation of Various Organic Substrates Using a NiO or CuO Nanocatalyst in the Presence of TBHP as the Oxidant and DMF as the Amine Source



identical reaction conditions, using NiO and CuO nanocatalysts (Scheme 3). Oxidative amidation of substituted benzaldehydes in the presence of NiO (Table 1, entries 1–7) showed moderate catalytic performance with low selectivity for the tertiary amides. The corresponding carboxylic acids were indeed formed as major byproducts during the catalytic reaction. Substituted carboxylic acids (Table 1, entries 8 and 9) showed poor catalytic performance with low conversions and moderate selectivity for *N,N*-dialkylated amides. Five-membered rings such as furfural (Table 1, entry 10) showed complete conversion but moderate (40%) selectivity for its *N,N*-dialkylated amide. 2-Thiophenecarboxylic acid (Table 1, entry 11) presented a better conversion (75%) and selectivity (51%) for the tertiary amide.

Owing to its better performance, also CuO was investigated to establish a broader reaction scope, including various substituted substrates (Scheme 3 and Table 2). Excellent conversions and selectivity toward tertiary amides were indeed obtained with BAs substituted with both electron-donating as well as electron-withdrawing groups attached to the aromatic ring (Table 2, entries 1–5). A similar trend was observed in the case of aldehydes and alcohols (Table 2, entries 6–17). Six-membered heterocyclic N-containing compounds, pyridin-2-ylmethanol and picolinic acid, gave excellent performance with CuO with high conversion and selectivity for *N,N*-dimethylpicolinamide (Table 2, entries 18 and 19). Five-membered heterocyclic compounds containing O and S atoms also gave promising results: furfural aldehyde presented 92% conversion and more than 97% selectivity for *N,N*-dimethylfuran-2-carboxamide; thiophene-2-carbaldehyde and thiophene-2-carboxylic acid showed 100% conversion with 93% and 97% selectivity, respectively, for *N,N*-dimethylthiophene-2-carboxamide (Table 2, entries 20–22).

After achieving promising catalytic activities of the CuO nanocatalyst toward alcohols, aldehydes, and acids, we further explored the catalytic activity of the CuO nanocatalyst toward unsaturated compounds under identical conditions (Table 3). To our surprise, phenyl acetylene gave complete conversion with the formation of *N,N*-dimethyl-2-phenylacetamide with 36% selectivity and 1 as a major byproduct (16%) via C–C bond cleavage (Table 3, entry 1). Phenylacetylene substituted with electron-donor groups at the para position was also investigated for catalytic transformation into tertiary amides. With the methyl group, no significant variation in the catalytic

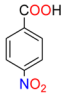
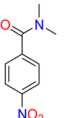
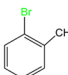
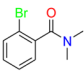
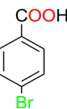
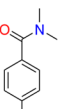
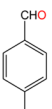
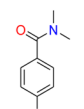
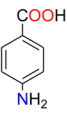
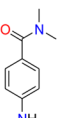
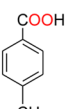
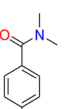
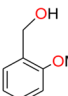
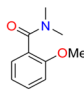
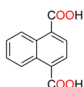
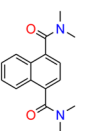
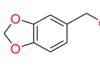
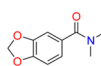
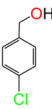
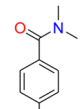
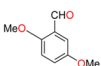
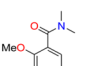
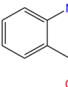
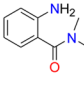
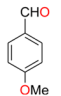
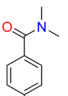
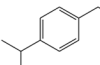
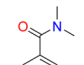
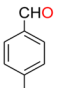
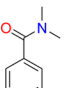
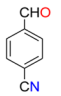
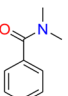
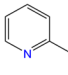
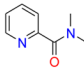
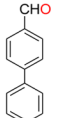
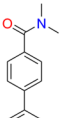
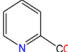
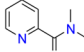
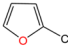
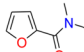
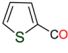
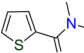
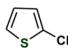
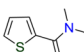
Table 1. Oxidative Amidation of Substituted Aldehydes and Acids Using a NiO Nanocatalyst^b

Entry	Substrate	% Con. ^a	Product (A) N,N-dialkylated amide	% Sel. ^a
Aldehydes				
1		89.5		43.4
2		82		46.8
3		78.3		70.9
4		88.3		63
5		72.4		40
6		97.5		74
7		97.5		47
Carboxylic acids				
8		15		62.6
9		14.4		34
Fivemembered ring				
10		100		40
11		75		50.8

^a% conversion and % selectivity were determined by GC–MS analysis.

^bReaction conditions: substrate = 1 mmol; TBHP = 6 equiv; catalyst = 10 mg; DMF = 2 g (2.12 mL); *T* = 80 °C; reaction time = 20 h.

Table 2. Oxidative Amidation of Substituted Aromatic Acids, Aldehydes, and Alcohols Using a CuO Nanocatalyst^b

Entry	Compound Name	% Con. ^a	Product (C) N,N-dimethylated amide	% Sel. ^a	Entry	Compound Name	% Con. ^a	Product (C) N,N-dimethylated amide	% Sel. ^a
Carboxylic acids									
1		100		69.2	11		58.3		98.4
2		100		100	12		81.4		98
3		100		29	Alcohols				
4		98.2		88	13		93.5		74.1
5		100		70	14		81		51.5
Aldehydes					15		70		58.9
6		81		70.3	16		100		52
7		96.7		62	17		93.7		55.2
8		100		92.2	heterocycles				
9		80.2		70	18		96.1		83
10		86.5		95.1	19		100		93
					20		92.3		97
					21		100		97
					22		100		93

^a% conversion and % selectivity were determined by GC–MS analysis. ^bReaction conditions: substrate = 1 mmol; TBHP = 6 equiv; catalyst = 10 mg; DMF = 2 g (2.12 mL); *T* = 80 °C; reaction time = 20 h.

performance was observed, but with the methoxy group, 2-(4-methoxyphenyl)-*N,N*-dimethylacetamide was obtained with

50% selectivity (Table 3, entries 2 and 3). Oxidative amidation of cinnamaldehyde gave *N,N*-dimethyl-2-phenylethanamine as

Table 3. Oxidative Amidation of Unsaturated Compounds Using a CuO Nanocatalyst^b

Entry	Compound Name	% Con. ^a	Product (D) % Sel. ^a	Product (E) % Sel. ^a
Unsaturated compounds				
1		100	 36	 16
2		100	 32	 16
3		100	 50	 18
4		100	 36	 32

^a% conversion and % selectivity were determined by GC–MS analysis.^bReaction conditions: substrate = 1 mmol; TBHP = 6 equiv; catalyst = 10 mg; DMF = 2 g (2.12 mL); *T* = 80 °C; reaction time = 20 h.

a major product (36%) and **1** as a major byproduct (32%) because of C–C bond cleavage (Table 3, entry 4).

On the basis of previous literature reports on the oxidation of alkynes and their transformation into amides,^{18,40} we have proposed a mechanism for the catalytic oxidation of alkynes to amides (Scheme S1).^{41–43} However, we were not able to trap chetene-based radicals, for example, by using TEMPO. On the other hand, the occurrence of oxidative cleavage of the $\text{C}\equiv\text{C}$ bond is demonstrated by an extensive amount of **1** as the major byproduct.

Catalytic oxidative amidation using a series of esters was performed using CuO nanoparticles prepared from SSMP-2. Unfortunately, the CuO nanoparticles were ineffective in catalyzing the conversion of esters to amides. Methylbenzoate showed 3% conversion with 100% selectivity for **1**. Oxidative amidation of ethyl 2-phenylacetate also showed poor conversion with 35% selectivity for **2** and 30% selectivity for *N,N*-dimethyl-2-phenylacetamide. Methyl 4-chlorobenzoate was found to be inert toward oxidative amidation under identical reaction conditions, whereas methyl 4-aminobenzoate showed 8% conversion with 100% selectivity for *N,N*-dimethyl-4-(*N*-methylformamido)benzamide (see Table S2). In the presence of CuO nanoparticles, oxidative amidation of --COOMe occurred along with *N*-formylation and *N*-alkylation of amine to form *N,N*-dimethyl-4-(*N*-methylformamido)-benzamide. Unfortunately, the product selectivity was low, and only 8% product was obtained (see Table S2).

Recycling studies were then performed to determine whether these heterogeneous nanocatalysts can be recycled and reused. NiO and CuO were thus used to investigate the oxidative amidation of benzaldehyde along several reaction runs (Figure 7A,B). Recycling studies clearly showed that NiO gives >95% benzaldehyde conversion and >68% selectivity for **1** for at least five cycles. The CuO nanocatalyst was also recyclable for at least six recycles for BA with >96% conversion and >75% selectivity for **1**. XPS experiments (Figures 5 and 6) and XRD (Figure 2) on the recovered nanocatalysts confirmed retention of both the composition and structure of their fresh catalysts, suggesting that, after recycling of the catalysts, no chemical modification or surface poisoning occurred (see the discussion above). Moreover, FESEM results for the spent catalysts also rule out aggregation of the particles, which retain their morphology, with only minor product adsorption.

Oxidative amidation of oxygenated organic compounds has been mostly investigated using homogeneous and heterogeneous transition-metal-based catalysts. A comparative study for the catalytic performance of various homogeneous and heterogeneous catalysts toward the formation of **1** is presented in Table S3. The CuO nanocatalyst displays excellent yield of **1**, starting from BA and DMF, using milder conditions and without additional solvents. The nanocatalysts used display several advantages with respect to the existing systems (see Table S3). Although there are several reports on homogeneous

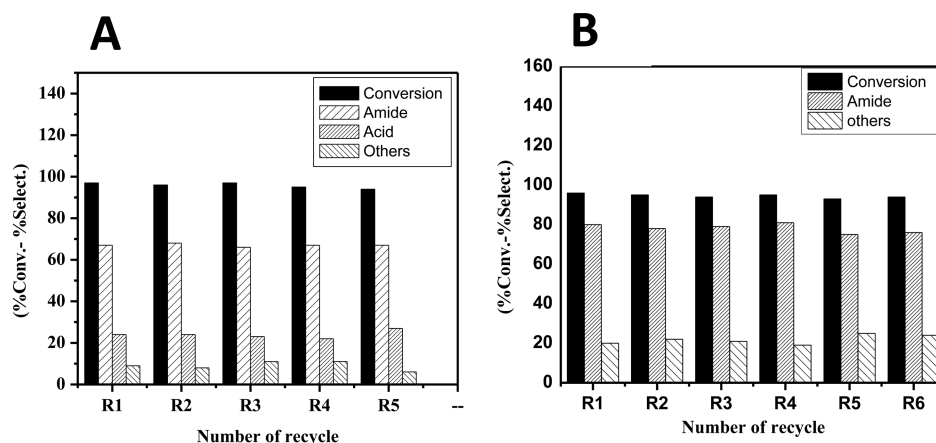


Figure 7. Recycling study for benzaldehyde with NiO (A) and CuO (B) nanocatalysts. Reaction conditions: substrate = 1 mmol; TBHP = 6 equiv; catalyst = 10 mg; DMF = 2 g (2.12 mL); *T* = 80 °C; reaction time = 20 h. % conversion and % selectivity were determined by GC–MS analysis; the catalysts were recovered via centrifugation of the reaction mixture after every reaction run (see the experimental details).

catalysts for oxidative amidation aimed at the synthesis of N-alkylated amides, these processes suffer from several drawbacks, such as poor recyclability, difficult catalyst recovery, the need for additional solvents, and the generation of copious amount of waste.⁴⁴ There are also some reports on heterogeneous metal-based catalysts for oxidative amidation reactions (Table S3). Although a heterogeneous Cu-based nanocatalyst was investigated for oxidative amidation,¹³ a broad substrate scope for such a catalyst was not established. Within this scenario, the CuO nanocatalyst represents an appealing and cost-effective alternative because it allows one to obtain N-alkylated amides, starting from several substrates, with higher selectivity, under milder conditions.

CONCLUSIONS

In summary, nickel and copper oxide nanocatalysts featuring spherical and rod-shaped morphology were procured by thermal decomposition of their respective SSMPs (SSMP-1 and SSMP-2). Molecular structures of SSMP-1 and SSMP-2 were annotated by X-ray crystallography. We have assiduously investigated the response of cobalt, nickel, and copper oxide-based nanoparticles toward oxidative amidation of various oxygenated and unsaturated organic compounds. Cobalt/cobalt oxide- and nickel oxide-based nanoparticles showed moderate catalytic performance for aldehydes and alcohols and poor catalytic performance for carboxylic acid. On the other hand, CuO nanoparticles had preponderance over other transition-metal-based oxide nanoparticles with an excellent catalytic performance for the oxidative amidation of oxygenates and unsaturated compounds with a broad reaction/substrate scope, under moderate reaction conditions. The studied nanocatalyst can be recycled, retaining high activity up to six runs with an unaffected performance. Oxidative amidation of various oxygenated, as well as unsaturated organic compounds, has been sparsely investigated at the nanoscale level because very few literature reports are accessible. The thorough investigation in the present work can, therefore, serves as a guide in the design of a catalytic material for the oxidative amidation of oxygenated and unsaturated organic compounds in the future. The present work demonstrates a perfect blend of inorganic and material chemistry by employing inorganic complexes as SSMPs for the synthesis of their respective metal oxide nanoparticles.

EXPERIMENTAL SECTION

Materials. Commercially available starting materials were used as received. $\text{NiSO}_4 \cdot 6\text{H}_2\text{O}$, $\text{Cu}(\text{CH}_3\text{COO})_2 \cdot \text{H}_2\text{O}$, benzoic acid (BA), and citric acid were purchased from Merck India. 2-(2-Hydroxyethyl)pyridine (hep-H), *tert*-butyl hydroperoxide (TBHP; 70 wt % in H_2O), *tert*-butyl peroxybenzoate, organic aldehydes, acids, and alcohols, phenylacetylene, and substituted phenylacetylene reagents were purchased from Sigma-Aldrich and other reagent grade solvents were used as received.

Physicochemical Characterizations. Powder XRD studies were carried out on Rigaku SmartLab X-ray diffractometer using $\text{Cu K}\alpha$ radiation (1.54 Å). IR spectra were performed on a Bio-Rad FTS 3000MX instrument using KBr pellets. FESEM in accordance with EDAX was done using a Supra 55 Zeiss field-emission scanning electron microscope. TEM was carried out on a FEI Tecnai G2 12 Twin transmission electron microscope. XPS analysis of fresh and spent catalysts (NiO and CuO) was performed using XPS with an auger electron spectroscopy (AES) module (model/supplier: PHI 5000 Versa Prob II, FEI Inc.). Identification of the products was carried out using a Shimadzu gas chromatograph–mass spectrometer equipped with a QP2010 mass spectrometer and a RTX-5 tubular

diphenyldimethylpolysiloxane capillary column [30 m in length, 0.25 mm in diameter, and with a df (film thickness) value of 1.0 μm].

X-ray Crystallographic Determination. Single-crystal X-ray structural studies of compounds were performed on a CCD-equipped Supernova diffractometer from Agilent Technologies with low-temperature equipment. The data for SSMP-1 and SSMP-2 were recorded using a Mo source. The strategy for the data collection was evaluated using *CrysAlisPro* CCD software. The data were collected by the standard ϕ – ω scan techniques and scaled and reduced using *CrysAlisPro* RED software. The structures were solved and refined by full-matrix least squares with *SHELXL-97*, refining on F^2 .⁴⁵ The positions of all of the atoms were obtained by direct methods. All non-H atoms were refined anisotropically. The remaining H atoms were placed in geometrically constrained positions and refined with isotropic temperature factors, generally $1.2U_{\text{eq}}$ of their parent atoms. All molecular drawings were obtained using the program *Diamond* (version 2.1d). The crystal and refinement data are summarized in Table S1.

Preparation of Single-Source Molecular Precursors (SSMPs): SSMP-1 and SSMP-2. Synthesis of SSMP-1. A methanolic solution of hep-H (0.123 g, 1.0 mmol, 15.0 mL) was prepared under continuous stirring conditions. To the aforementioned solution was added dropwise a $\text{NiSO}_4 \cdot 6\text{H}_2\text{O}$ (0.262 g, 1.0 mmol, 15.0 mL) methanolic solution, and the resultant mixture was stirred magnetically for 6 h at 298 K. The resulting solution was then passed through filter paper to remove unreacted solid. The filtrate was allowed to stand at room temperature for crystallization. Green block-shaped crystals of SSMP-1 appeared within a week by slow evaporation of the solvent. A suitable X-ray-quality crystal was then subjected to X-ray analysis, which confirmed the identity of the crystal as SSMP-1.

SSMP-1. FT-IR (KBr, cm^{-1}): 3280(br), 2905(w), 1615(m), 1489(m), 1434(m), 1371(m), 1114(s), 1028(m), 861(m), 766(w), 766(m), 623(m), 577(m).

Synthesis of SSMP-2. A total of 15 mL of a hep-H (0.123 g, 1.0 mmol) and BA (0.122 g, 1.0 mmol) solution was prepared in acetonitrile. To this was added dropwise a solution of copper acetate with acetonitrile (0.199 g, 1.0 mmol, 15.0 mL), and the resultant mixture was stirred magnetically for 8 h at 298 K. The resulting mixture was then passed through filter paper to remove unreacted solid. The filtrate was allowed to stand at room temperature for crystallization. Blue block-shaped crystals of SSMP-2 appeared within 10 days upon slow evaporation of the solvent. A suitable X-ray-quality crystal was then subjected to X-ray analysis, which confirmed the identity of the crystal as SSMP-2.

SSMP-2. FT-IR (KBr, cm^{-1}): 3425(br), 2924(m), 2802(w), 1615(s), 1562(m), 1395(s), 1257(m), 1111(m), 1066(s), 1030(m), 769(m), 721(m), 682(m), 618(m).

Note: For application purposes, bulk SSMP-1 and SSMP-2 were also prepared, and the yields (%) were calculated and found to be 91% and 80%, respectively.

Synthesis of CoNC via a Reduction Method. CoNC was prepared by reduction of the SSMP $[\text{Co}^{\text{II}}(\text{hep-H})(\text{H}_2\text{O})_4]\text{SO}_4$ [A; hep-H = 2-(2-hydroxyethyl)pyridine] using NaBH_4 as the reducing agent. A detailed synthetic procedure and characterization of SSMP (A) and CoNC were previously reported.^{29,32}

Synthesis of a Nanocatalyst (NiO or CuO) via Sol–Gel-Assisted Thermal Decomposition of Their SSMPs. The synthesis of a nanocatalyst was carried out using sol–gel-assisted thermal decomposition of SSMP-1 or SSMP-2. In a typical synthesis of the nanocatalyst, SSMP-1 or SSMP-2 (10.0 mmol) was dissolved in 100 mL of distilled water under vigorous stirring at 80 °C. The pH of the reaction mixture was maintained at nearly 2.0–2.5 using citric acid (1.0 M). After complete dissolution of the SSMP, under continuous stirring and heating, the diluted solution (sol) became a concentrated solution (gel), which, upon an increase in the temperature at around 140 °C in 45 min, further leads to the formation of a fluffy-like black solid. The latter was transferred to a 500 °C furnace in order to obtain the pure and crystalline phase of black NiO or CuO nanocatalysts.

General Procedure for the Catalytic Reactions. The liquid-phase catalytic oxidations were carried out in a 25 mL two-neck,

round-bottomed flask equipped with a magnetic stirrer and immersed in a thermostated oil bath. The flask was charged with a substrate (1 mmol), TBHP as the oxidant (6 equiv added as 70 wt % H₂O), 10 mg of catalyst, and 2 g (2.12 mL) of the solvent DMF. All of the reactions were carried out at *T* = 80 °C. At the end of the reaction, 10 mol % dodecane was added with respect to the substrate as an internal standard. Then, the catalyst was separated via centrifugation, and a sample of the liquid mixture was periodically subjected to GC–MS analysis. The calibration was done using 10 mol % dodecane, with respect to the substrate, as the internal standard. After completion, the reaction mixture was diluted with water and extracted with ethyl acetate (100 mL of ethyl acetate, three times). The combined organic phase was dried over anhydrous sodium sulfate, and the solvent was removed using a rotavapor. For benzyl alcohol, benzaldehyde, and BA using CuO nanoparticles, a pure product was obtained by flash column chromatography (1:1 ethyl acetate/hexane as the eluent). Isolated yields obtained from column chromatography matched the results obtained from GC–MS.

■ ASSOCIATED CONTENT

■ Supporting Information

The Supporting Information is available free of charge on the ACS Publications website at DOI: 10.1021/acs.inorgchem.7b01576.

Crystallographic information for SSMP-1 (CCDC 1048646) and SSMP-2 (CCDC 1511656), FT-IR spectral characterization images including other supporting XPS spectra and SEM images for NiO and CuO nanocatalysts, GC–MS data, and NMR spectra (PDF)

Accession Codes

CCDC 1048646 and 1511656 contain the supplementary crystallographic data for this paper. These data can be obtained free of charge via www.ccdc.cam.ac.uk/data_request/cif, or by emailing data_request@ccdc.cam.ac.uk, or by contacting The Cambridge Crystallographic Data Centre, 12 Union Road, Cambridge CB2 1EZ, UK; fax: +44 1223 336033.

■ AUTHOR INFORMATION

Corresponding Author

*E-mail: xray@iiti.ac.in. Tel: 91-731-2438 752.

ORCID

Shaikh M. Mobin: 0000-0003-1940-3822

Notes

The authors declare no competing financial interest.

■ ACKNOWLEDGMENTS

S.M.M. thanks SERB-DST (Project EMR/2016/001113), New Delhi, India, and IIT Indore for financial support. We are also grateful to Reshma S. Kokane from the CSIR National Chemical Laboratory, Pune, India, for providing TEM data. We also acknowledge the Advanced Center for Materials Science and Material Science & Engineering, IIT Kanpur, for XPS and microscopic characterization facility, respectively. A.M. and T.G. are grateful to the MHRD, Government of India, for a research fellowship and SIC, IIT Indore, for providing the characterization facility. P.C. is grateful to the MEMS, IIT Indore, for providing a fellowship.

■ REFERENCES

(1) Tan, B.; Toda, N.; Barbas, C. F. Organocatalytic Amidation and Esterification of Aldehydes with Activating Reagents by a Cross-Coupling Strategy. *Angew. Chem., Int. Ed.* **2012**, *51*, 12538–12541.

(2) Kuranaga, T.; Sesoko, Y.; Inoue, M. Cu-mediated Enamide Formation in the Total Synthesis of Complex Peptide Natural Products. *Nat. Prod. Rep.* **2014**, *31*, 514–532.

(3) Al-Zoubi, R. M.; Marion, O.; Hall, D. G. Direct and Waste-Free Amidations and Cycloadditions by Organocatalytic Activation of Carboxylic Acids at Room Temperature. *Angew. Chem.* **2008**, *120*, 2918–2921.

(4) Wang, H.; Guo, L.-N.; Duan, X.-H. Copper-catalyzed Oxidative Condensation of α -oxocarboxylic Acids with Formamides: Synthesis of α -ketoamides. *Org. Biomol. Chem.* **2013**, *11* (28), 4573–4576.

(5) Jiang, H.; Lin, A.; Zhu, C.; Cheng, Y. Copper-catalyzed C–N Bond Formation through C–H/N–H Activation: A Novel Approach to the Synthesis of Multisubstituted Ureas. *Chem. Commun.* **2013**, *49*, 819–821.

(6) Hosoi, K.; Nozaki, K.; Hiyama, T. Carbon monoxide Free Aminocarbonylation of Aryl and Alkenyl Iodides using DMF as an Amide Source. *Org. Lett.* **2002**, *4*, 2849–2851.

(7) Ju, J.; Jeong, M.; Moon, J.; Jung, H. M.; Lee, S. Amino-carbonylation of Aryl Halides Using a Nickel Phosphite Catalytic System. *Org. Lett.* **2007**, *9*, 4615–4618.

(8) Owston, N. A.; Parker, A. J.; Williams, J. M. Highly efficient ruthenium-catalyzed oxime to amide rearrangement. *Org. Lett.* **2007**, *9*, 3599–3601.

(9) Yavari, I.; Ghazanfarpour-Darjani, M.; Bayat, M. J. Synthesis of Amides via Copper-Catalyzed Amidation of Aryl Halides Using Isocyanides. *Tetrahedron Lett.* **2014**, *55*, 4981–4982.

(10) Li, Y.; Zhu, F.; Wang, Z.; Wu, X.-F. Copper-Catalyzed Carbonylative Synthesis of Aliphatic Amides from Alkanes and Primary Amines via C_(sp3)–H Bond Activation. *ACS Catal.* **2016**, *6*, 5561–5564.

(11) (a) Azizi, K.; Karimi, M.; Nikbakht, F.; Heydari, A. Direct Oxidative Amidation of Benzyl Alcohols using EDTA@Cu(II) Functionalized Superparamagnetic Nanoparticles. *Appl. Catal., A* **2014**, *482*, 336–343. (b) Bilyachenko, A. N.; Dronova, M. S.; Yalymov, A. I.; Lamaty, F.; Bantreil, X.; Martinez, J.; Bizet, C.; Shul'pina, L. S.; Korlyukov, A. A.; Arkhipov, D. E.; Levitsky, M. M.; Shubina, E. S.; Kirillov, A. M.; Shul'pin, G. B. Cage-like Copper(II) Silsesquioxanes: Transmetalation Reactions and Structural, Quantum Chemical, and Catalytic Studies. *Chem. - Eur. J.* **2015**, *21*, 8758–8770. (c) Gaspa, S.; Porcheddu, A.; De Luca, L. Iron-catalysed oxidative amidation of alcohols with amines. *Org. Biomol. Chem.* **2013**, *11*, 3803–3807. (d) Bilyachenko, A. N.; Levitsky, M. M.; Yalymov, A. I.; Korlyukov, A. A.; Vologzhanina, A. V.; Kozlov, Y. N.; Shul'pina, L. S.; Nesterov, D. S.; Pombeiro, A. J. L.; Lamaty, F.; Bantreil, X.; Fetre, A.; Liu, D.; Martinez, J.; Long, J.; Larionova, J.; Guari, Y.; Trigub, A. L.; Zubavichus, Y. V.; Golub, I. E.; Filippov, O. A.; Shubina, E. S.; Shul'pin, G. B. A heterometallic (Fe₆Na₈) cage-like silsesquioxane: synthesis, structure, spin glass behavior and high catalytic activity. *RSC Adv.* **2016**, *6*, 48165–48180. (e) Bilyachenko, A. N.; Levitsky, M. M.; Yalymov, A. I.; Korlyukov, A. A.; Khrustalev, V. N.; Vologzhanina, A. V.; Shul'pina, L. S.; Ikonnikov, N. S.; Trigub, A. E.; Dorovatovskii, P. V.; Bantreil, X.; Lamaty, F.; Long, J.; Larionova, J.; Golub, I. E.; Shubina, E. S.; Shul'pin, G. B. Cage-like Fe₆Na₈-Germesquioxanes: Structure, Magnetism, and Catalytic Activity. *Angew. Chem., Int. Ed.* **2016**, *55*, 15360–15363. (f) Yalymov, A. I.; Bilyachenko, A. N.; Levitsky, M. M.; Korlyukov, A. A.; Khrustalev, V. N.; Shul'pina, L. S.; Dorovatovskii, P. V.; Es'kova, M. A.; Lamaty, F.; Bantreil, X.; Villemejeanne, B.; Martinez, J.; Shubina, E. S.; Kozlov, Y. N.; Shul'pin, G. B. *Catalysts* **2017**, *7*, 101. (g) Wu, X.-F.; Sharif, M.; Pews-Davtyan, A.; Langer, P.; Ayub, K.; Beller, M. The First Zn^{II}-Catalyzed Oxidative Amidation of Benzyl Alcohols with Amines under Solvent-Free Conditions. *Eur. J. Org. Chem.* **2013**, *2013*, 2783–2787.

(12) Hu, C.; Yan, X.; Zhou, X.; Li, Z. Copper-Catalyzed Formation of N, N-dimethyl Benzamide From Nitrile and DMF Under an O₂ Atmosphere. *Org. Biomol. Chem.* **2013**, *11*, 8179–8182.

(13) Saberi, D.; Mahdudi, S.; Cheraghi, S.; Heydari, A. Cu(II)–acetylacetone Complex Covalently Anchored onto Magnetic Nanoparticles: Synthesis, Characterization and Catalytic Evaluation in Amide Bond Formation via Oxidative Coupling of Carboxylic Acids

with N,N-dialkylformamides. *J. Organomet. Chem.* **2014**, 772–773, 222–228.

(14) Bai, C.; Yao, X.; Li, Y. Easy Access to Amides through Aldehydic C–H Bond Functionalization Catalyzed by Heterogeneous Co-based Catalysts. *ACS Catal.* **2015**, 5, 884–891.

(15) Feng, J.-B.; Wei, D.; Gong, J.-L.; Qi, X.; Wu, X.-F. Oxidative Synthesis of Benzamides From Toluenes and DMF. *Tetrahedron Lett.* **2014**, 55, 5082–5084.

(16) Bao, Y.-S.; Wang, L.; Jia, M.; Xu, A.; Agula, B.; Baiyin, M.; Zhaorigetu, B. Heterogeneous Recyclable Nano-palladium Catalyzed Amidation of Esters Using Formamides as Amine Sources. *Green Chem.* **2016**, 18, 3808–3814.

(17) Xu, K.; Hu, Y.; Zhang, S.; Zha, Z.; Wang, Z. Direct Amidation of Alcohols with N-Substituted Formamides under Transition-Metal-Free Conditions. *Chem. - Eur. J.* **2012**, 18, 9793–9797.

(18) Kim, I.; Lee, C. Rhodium-Catalyzed Oxygenative Addition to Terminal Alkynes for the Synthesis of Esters, Amides, and Carboxylic Acids. *Angew. Chem., Int. Ed.* **2013**, 52, 10023–10026.

(19) Ghosh, S. C.; Ngiam, J. S.; Chai, C. L.; Seayad, A. M.; Dang, T. T.; Chen, A. Iron-Catalyzed Efficient Synthesis of Amides from Aldehydes and Amine Hydrochloride Salts. *Adv. Synth. Catal.* **2012**, 354, 1407–1412.

(20) Fudjda, K. L.; Tilley, T. D. Dimolybdenum (III) Complexes of $\text{OSi}(\text{O}t\text{Bu})_3\text{-O}_2\text{P}(\text{O}t\text{Bu})_2$ and $\text{-OB}[\text{OSi}(\text{O}t\text{Bu})_3]_2$ as Single-Source Molecular Precursors to Molybdenum-Containing, Multi-Component Oxide Materials. *Chem. Mater.* **2004**, 16, 1035–1047.

(21) Zhao, L.; Yosef, M.; Pippel, E.; Hofmeister, H.; Steinhart, M.; Goesele, U.; Schlecht, S. Four Birds with One Stone: Synthesis of Nanostructures of ZnTe , Te , ZnAl_2O_4 , and $\text{Te/ZnAl}_2\text{O}_4$ from a Single-Source Precursor. *Angew. Chem., Int. Ed.* **2006**, 45, 8042–8045.

(22) Cowley, A. H.; Jones, R. A. Single-Source III/V Precursors: A New Approach to Gallium Arsenide and Related Semiconductors. *Angew. Chem., Int. Ed. Engl.* **1989**, 28, 1208–1215.

(23) Zaera, F. Nanostructured materials for applications in heterogeneous catalysis. *Chem. Soc. Rev.* **2013**, 42, 2746–2762.

(24) Fudjda, K. L.; Tilley, T. D. Design and Synthesis of Heterogeneous Catalysts: the Thermolytic Molecular Precursor Approach. *J. Catal.* **2003**, 216, 265–275.

(25) Saha, K.; Agasti, S. S.; Kim, C.; Li, X.; Rotello, V. M. Gold Nanoparticles in Chemical and Biological Sensing. *Chem. Rev.* **2012**, 112, 2739–2779.

(26) Boschloo, G.; Hagfeldt, A. Spectroelectrochemistry of Nanostructured NiO. *J. Phys. Chem. B* **2001**, 105, 3039–3044.

(27) Xie, X.; Li, Y.; Liu, Z.-Q.; Haruta, M.; Shen, W. Low-temperature Oxidation of CO Catalysed by Co_3O_4 Nanorods. *Nature* **2009**, 458, 746–749.

(28) Park, J.; Kang, E.; Son, S. U.; Park, H. M.; Lee, M. K.; Kim, J.; Kim, K. W.; Noh, H. J.; Park, J. H.; Bae, C. J.; Park, J.-G.; Hyeon, T. Monodisperse Nanoparticles of Ni and NiO: Synthesis, Characterization, Self-Assembled Superlattices, and Catalytic Applications in the Suzuki Coupling Reaction. *Adv. Mater.* **2005**, 17, 429–434.

(29) Mohammad, A.; Mishra, V.; Chandra, P.; Mobin, S. M. Reduction of Selective Polyaromatic Nitrotritycene via Azoxytritycene Intermediate under Ambient Conditions Using Cobalt/Cobalt Oxide Nanocomposite (CoNC). *RSC Adv.* **2016**, 6, 60602–60608.

(30) Brutchey, R. L.; Lugmair, C. G.; Schebaum, L. O.; Tilley, T. D. Thermolytic Conversion of a Bis (alkoxy) Tris (siloxo) Tantalum (V) Single-source Molecular Precursor to Catalytic Tantalum-silica Materials. *J. Catal.* **2005**, 229, 72–81.

(31) Brutchey, R. L.; Mork, B. V.; Sirbulu, D. J.; Yang, P.; Tilley, T. D. A Dimeric Molecular Precursor $[(t\text{BuO})_2\text{Ti}\{\mu\text{-O}_2\text{Si}[\text{OSi}(\text{O}t\text{Bu})_3]_2\}]_2$ to Ti (IV)/ SiO_2 catalysts for selective cyclohexene epoxidation. *J. Mol. Catal. A: Chem.* **2005**, 238, 1–12.

(32) Mobin, S. M.; Mohammad, A. Retention of single crystals of two Co (II) complexes during chemical reactions and rearrangement. *Dalton Trans.* **2014**, 43, 13032–13040.

(33) Danks, A.; Hall, S.; Schnepf, Z. The Evolution of ‘Sol-gel’ Chemistry as a Technique for Materials Synthesis. *Mater. Horiz.* **2016**, 3, 91–112.

(34) Dong, C.; Xiao, X.; Chen, G.; Guan, H.; Wang, Y.; Djerdj, I. Porous NiO Nanosheets Self-grown on Alumina Tube Using a Novel Flash Synthesis and Their Gas Sensing Properties. *RSC Adv.* **2015**, 5, 4880–4885.

(35) Langford, J. I.; Wilson, A. J. C. Scherrer after Sixty Years: A Survey and Some New Results in the Determination of Crystallite Size. *J. Appl. Crystallogr.* **1978**, 11, 102–113.

(36) Zhao, B.; Liu, P.; Zhuang, H.; Jiao, Z.; Fang, T.; Xu, W.; Lu, B.; Jiang, Y. Hierarchical Self-assembly of Microscale Leaf-like CuO on Graphene Sheets for High-Performance Electrochemical Capacitors. *J. Mater. Chem. A* **2013**, 1, 367–373.

(37) Peck, M. A.; Langell, M. A. Comparison of Nanoscaled and Bulk NiO Structural and Environmental Characteristics by XRD, XAFS, and XPS. *Chem. Mater.* **2012**, 24, 4483–4490.

(38) Dubale, A. A.; Pan, C.-J.; Tamirat, A. G.; Chen, H.-M.; Su, W.-N.; Chen, C.-H.; Rick, J.; Ayele, D. W.; Aragaw, B. A.; Lee, J.-F.; Yang, Y.-W.; Hwang, B.-J. Heterostructured $\text{Cu}_2\text{O/CuO}$ Decorated with Nickel as a Highly Efficient Photocathode for Photoelectrochemical Water Reduction. *J. Mater. Chem. A* **2015**, 3, 12482–12499.

(39) Albert-Soriano, M.; Pastor, I. M. Metal–Organic Framework Based on Copper and Carboxylate-Imidazole as Robust and Effective Catalyst in the Oxidative Amidation of Carboxylic Acids and Formamides. *Eur. J. Org. Chem.* **2016**, 2016, 5180–5188.

(40) Zeng, M.; Herzon, S. B. Synthesis of 1, 3-Amino Alcohols, 1, 3-Diols, Amines, and Carboxylic Acids from Terminal Alkynes. *J. Org. Chem.* **2015**, 80, 8604–8618.

(41) Allen, A. D.; Cheng, B.; Fenwick, M. H.; Givehchi, B.; Henry-Riyad, H.; Nikolaev, V. A.; Shikhova, E. A.; Tahmassebi, D.; Tidwell, T. T.; Wang, S. Ketene Reactions with the Aminoxyl Radical TEMPO: Preparative, Kinetic, and Theoretical Studies. *J. Org. Chem.* **2001**, 66, 2611–2617.

(42) Curci, R.; Fiorentino, M.; Fusco, C.; Mello, R.; Ballistreri, F. P.; Failla, S.; Tomaselli, G. A. Oxidation of Alkynes by Dioxiranes. *Tetrahedron Lett.* **1992**, 33, 7929–7932.

(43) Zeller, K.-P.; Kowalik, M.; Haiss, P. The Dimethyldioxirane-mediated Oxidation of Phenylethyne. *Org. Biomol. Chem.* **2005**, 3, 2310–2318.

(44) Cole-Hamilton, D. J. Homogeneous Catalysis—New Approaches to Catalyst Separation, Recovery and Recycling. *Science* **2003**, 299, 1702–1706.

(45) Sheldrick, G. M. *Acta Crystallogr., Sect. A* **2008**, A64, 112–122. Program for Crystal Structure Solution and Refinement; University of Göttingen: Göttingen, Germany, 1997.